First imaging results with the new generation of the KIT 3D Ultrasound Tomography device

T. Hopp, M. Zapf, L. Fernandez-Lago, F. Feldbusch, H. Gemmeke, and N.V. Ruiter

Karlsruhe Institute of Technology, Institute for Data Processing and Electronics, Germany

ABSTRACT

Ultrasound Tomography (USCT) is an emerging technology for early breast cancer detection. At Karlsruhe Institute of Technology we recently realized a new generation of full 3D USCT device with a pseudo-randomly sampled hemispherical aperture. In this paper we summarize first imaging results with phantoms and first volunteer images. Using a gelatin phantom with PVC inclusions we evaluated transmission imaging, which showed a deviation from the ground truth of less than $5\,m/s$ in the sound speed and $0.2\,dB/cm$ in the attenuation for the phantom body and less than $15\,m/s$ and $0.2\,dB/cm$ for an inclusion with a diameter of $2.2\,cm$. Geometric errors are in average in the range of $0.2\,cm$. For reflectivity imaging we showed that the point spread function is nearly isotropic and with an average of $0.26\,mm$ close to the theoretical predictions for the current system. While the system is still in final commissioning, the results of the phantom and volunteer imaging are very promising: after further calibration and deeper analysis with phantoms we aim at starting a clinical study.

Keywords: 3D Ultrasound tomography, reflectivity imaging, sound speed imaging, attenuation imaging, phantom study

1. INTRODUCTION

Ultrasound Tomography (USCT) is an emerging technology for early breast cancer detection. 2D and 2.5D USCT systems[1,2] have recently been approved for clinical use. At Karlsruhe Institute of Technology we focus on the design and realization of a 3D USCT system with a hemispherical aperture and unfocussed emission and reception in 3D. After having realized a first prototype for clinical studies,[3] we recently redesigned the system by – among others – enlarging the aperture for better illumination and larger field of view, adding a new patient interface aimed at imaging up to the chest wall, a pseudo-random distribution of transducers to reduce artifacts due to the sparsity of the system, and a faster data readout.[4] In this paper we follow up on the qualitative and quantitative evaluation of the image quality of the new system called 3D USCT III. We summarize first imaging results with phantoms and present a first analysis of volunteer images.

2. METHODS

2.1 System description

The imaging system of USCT III consists of a water filled hemispherical aperture with a diameter of $35.8\,cm$. On the inner surface of this aperture 128 transducer arrays system (TAS) with 18 transducers each are mounted. Each transducer may act as emitter and receiver. The locations of the transducers within one TAS are pseudo-randomized. While all TAS have the same pseudo-random distribution to facilitate automated production, the TAS are randomly rotated in the aperture to provide an overall pseudo-random distribution of the in total 2304 transducers. The measured center frequency of the transducers is $2.6 \pm 0.2\,MHz$ at a bandwidth of $3.4 \pm 0.2\,MHz$ at $-10\,dB$. The opening angle is 42.8 ± 0.8^o at $-10\,dB$. To acquire the signal raw data a dedicated data acquisition system with 384 parallel channels is used. Signals are digitized at $20\,MHz$ and 12 Bit, before they are stored in the on-board RAM (up to $96\,GB$). In order to increase the spatial sampling, the aperture can be rotated and translated.

To acquire the necessary raw data for offline image reconstruction, all permutations of emitting and receiving transducers are recorded, i.e. sequentially one transducer emits an ultrasound wave into the aperture, while all

Contact: torsten.hopp@kit.edu

other transducers record the scattered and transmitted wave. For exciting the transducers we used frequency coded chirp signals to allow recognition of the signals in the receiver with high suppression of noise and interference signals.

2.2 Image reconstruction

For transmission reconstruction we apply travel time tomography which assumes the wave propagation along rays. In a first step, the raw data for reconstruction is selected based on the opening angle of the transducers, see section 2.1, i.e. only data acquired by receivers on the opposite side of the aperture and which are in the main lobe of the emitting transducer are used. These signals are matched filtered with the excitation pulse to enhance the signal-to-noise-ratio (SNR) and compensate electronic offsets before a time windowing is applied, which restricts the signal to the expected time of flight from emitter to receiver assuming a lower and upper limit for the sound speed in the medium. Then the time of flight from emitters to receivers is detected by a correlation of the signal with an according signal from a measurement through water only. The resulting delay b is used to reconstruct the deviation from the sound speed in water using an algebraic reconstruction technique, which describes the image reconstruction as a linear equation system

$$Mx = b \tag{1}$$

in which x is the slowness in each voxel, i.e. the reconstructed image, and M is the system matrix describing the rays from emitters to receivers. These rays are initially connecting emitters and receivers on straight lines and may subsequently be refined by respecting refraction at tissue interfaces by introducing bent rays based on solving the Eikonal equation. The equation system is iteratively solved with a total variation minimization algorithm (TVAL3[5]), which inquires two regularization parameters μ and β representing the data fidelity and the smoothness of the solution respectively. To reduce artifacts we filter out obvious misdetections in delays which may be caused by low SNR in signals or malfunctioning transducers.

Using the same reconstruction method, b can be replaced by the attenuation of the signals, which we extract by comparing the energy of the transmission signal in the measurement with object to the measurement through water only. This is achieved by integrating over the envelope of the transmission signal in a time window given by the estimated time of flight and the pulse length.

For reflection reconstruction we apply synthetic aperture focusing technique (SAFT). Again the data is selected geometrically to use only back reflections to the side of the hemisphere at which the emitting transducer is located. Signals are processed by a matched filter using the excitation pulse. Then the transmission signal is removed before a detection of local maxima and a convolution with an optimal pulse is performed. According to the SAFT principle the time of arrival of reflections is calculated based on the sound speed image for phase aberration correction. The distance between emitter and voxel to be reconstructed respectively the voxel and the receiver are calculated and divided by the average sound speed either in water or along a traced path through the reconstructed sound speed volume. At this time of flight the amplitude in the corresponding is read and accumulated in the voxel. Repeating this principle for a lot of emitter-receiver combination results in an intensity contrast forming the image. The method has been parallelized on a multi-GPU system.[6]

2.3 Evaluation methods

To evaluate the image quality of transmission tomography we built a custom phantom consisting of a main body made from gelatin ($15\,g$ per $100\,ml$ water), which was molded in a Vaseline coated plastic cup. Within the gelatin we included four spherical inclusions made from Polyvinyl chloride (PVC) and Dioctyl Terephthalate (softener, $26\,g$ PVC powder per $150\,ml$ of softener). The defined sizes from 0.8 to $2.2\,cm$ of the inclusions was ensured by pouring the hot PVC material into a mold and slowly cooling it down to room temperature over 24 hours (Figure 1 left).

The ground truth for sound speed and attenuation was measured with a dedicated setup consisting of two opposing ultrasound transducers in a water bath.[7] The speed of sound and attenuation was measured as $1530\,m/s$ ($\pm$ approx. $10\,m/s$ at 20^oC) and $0.4\,dB/cm$ ($\pm$ approx. $0.1\,dB/cm$) in gelatin and $1430\,m/s$ ($\pm$ approx. $2\,m/s$

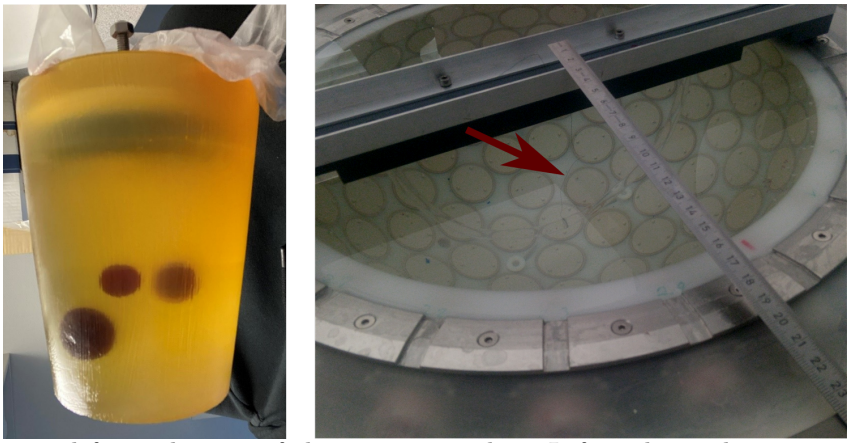

Figure 1: Phantoms used for evaluation of the imaging quality. Left: gelatin phantom with PVC inclusions. Right: Twisted bonding thread (see head of red arrow) in the 3D USCT III aperture.

at 20^oC) and $5.9\,dB/cm$ ($\pm$ approx. $0.5\,dB/cm$) in the PVC inclusions (Table 1). The attenuation was estimated as broadband attenuation for the USCT III transducer characteristics and the used excitation pulse.

After optimization of the regularization parameters μ and β by analyzing visibility of the inclusions, we investigated the agreement of sound speed respectively attenuation with the ground truth by taking the average respectively median value in a region of interest, which was manually positioned in the image. For the gelatin body the region of interest was a bounding box manually positioned in an area of the phantom in which no inclusion was visible. For the inclusions we manually annotated their center point in the image and set the region of interest by a sphere around that center point with a diameter equaling the ground truth. Furthermore we analyzed the agreement of the size of the inclusions by manually measuring the diameter of the inclusion along the x, y and z-axis in the reconstructed image.

To evaluate the point spread function in reflectivity imaging we used a twisted bonding wire with a diameter of $0.2\,mm$ (Figure 1 right). In the reconstructed images we selected slices which are approximately perpendicular to the surface of the wire in order to extract one-dimensional intensity profiles along the x-, y- and z-axis, on which the full width at half maximum (FWHM) could be calculated each.

Finally, we imaged first volunteers and visually assess the depth of the breast in the water bath, the visibility of the chest wall compared to our previous 3D USCT device, as well as the overall visibility of structures.

3. RESULTS

Figure 2 shows slices through the reconstructed transmission phantom. After optimization of the regularization parameters ($\mu = 200$, $\beta = 1$) all inclusions were visible in both the sound speed and attenuation image. To assess the repeatability of measurements, we imaged the phantom twice at two different positions in the aperture. The reconstructed sound speed of the gelatin was $1531.3\,m/s$ resp. $1526.4\,m/s$ compared to $1530\,m/s$ ground truth. The largest inclusion with a diameter of $2.2\,cm$ showed a sound speed of $1445.3\,m/s$ and $1436.1\,m/s$ compared to $1430\,m/s$ ground truth. The smaller inclusions down to $0.8\,cm$ had larger deviations of up to $70\,m/s$, however could still be distinguished from the background. The reason for the increasing error may partly be attributed to the blurring effect of the regularization and the finite position resolution, i.e. background voxels which are part of the phantom body with higher sound speed are increasingly getting part of the calculation of the average sound speed value. The reconstructed attenuation of the gelatin was $0.62\,dB/cm$ and $0.64\,dB/cm$ compared to $0.4\,dB/cm$ ground truth. The largest inclusion with a diameter of $2.2\,cm$ showed an attenuation of $6.1\,dB/cm$ and $5.8\,dB/cm$ compared to $5.9\,dB/cm$ ground truth. The values for both image acquisitions are in good agreement, indicating a good repeatability.

The absolute geometric error defined by the deviation of the diameter of inclusions from the ground truth was in average $0.2\,cm$ in sound speed and $0.1\,cm$ in attenuation for the largest $2.2\,cm$ inclusion. The error did

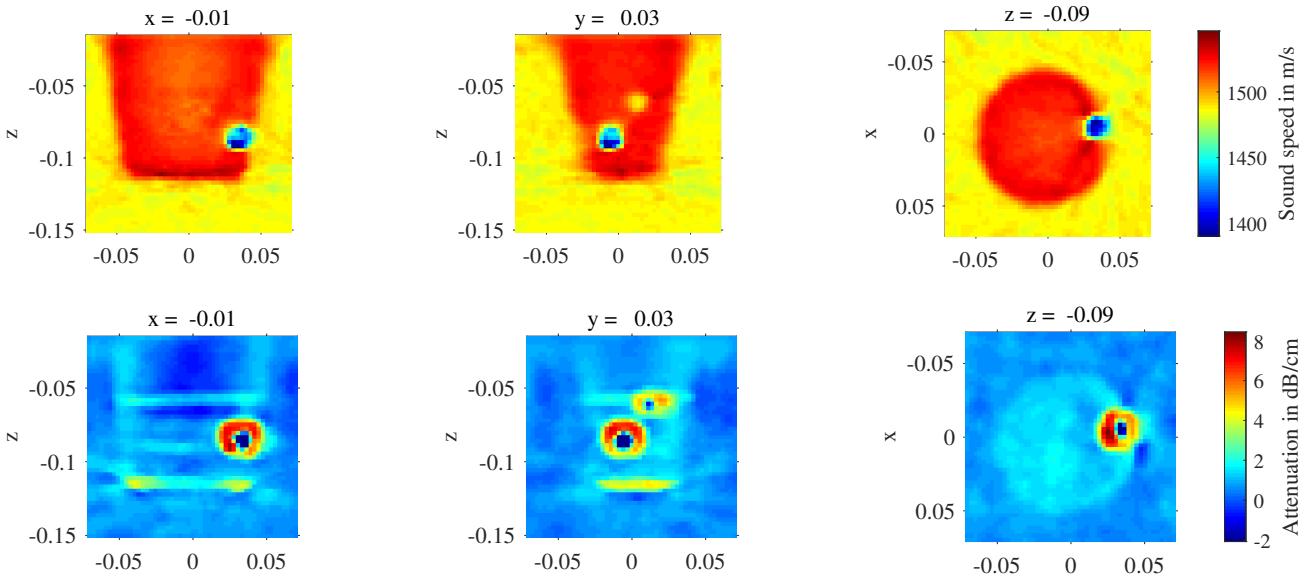

Figure 2: Sound speed (top) and attenuation (bottom) reconstruction of the gelatin phantom with PVC inclusions ($\mu = 200$, $\beta = 1$). The views from left to right show transversal, sagittal and coronal planes of the reconstructed volume.

	Ground truth		**Measurement position 1**		**Measurement position 2**	
	Sound speed	Attenuation	Sound speed	Attenuation	Sound speed	Attenuation
Gelatin	$1530 \pm 10 m/s$	$0.4 \pm 0.1 dB/cm$	$1531.2 m/s$	$0.64 dB/cm$	$1526.4 m/s$	$0.62 dB/cm$
PVC inclusion (2.2cm)	$1430 \pm 2 m/s$	$5.9 \pm 0.5 dB/cm$	$1445.3 m/s$	$6.10 dB/cm$	$1436.1 m/s$	$5.80 dB/cm$
PVC inclusion (1.7cm)	$1430 \pm 2 m/s$	$5.9 \pm 0.5 dB/cm$	$1381.5 m/s$	$4.80 dB/cm$	$1393.5 m/s$	$4.80 dB/cm$
PVC inclusion (1.2cm)	$1430 \pm 2 m/s$	$5.9 \pm 0.5 dB/cm$	$1453.3 m/s$	$3.40 dB/cm$	$1457.4 m/s$	$3.10 dB/cm$
PVC inclusion (0.8cm)	$1430 \pm 2 m/s$	$5.9 \pm 0.5 dB/cm$	$1500.4 m/s$	$3.00 dB/cm$	$1492.5 m/s$	$2.70 dB/cm$

Table 1: Summary of measurements for sound speed and attenuation in the custom phantom. The ground truth was measured a dedicated setup, see section 2.3. The measurement position 1 and measurement position 2 provide the measured values in the reconstructed images of the phantom imaged at two different positions within the 3D USCT III aperture.

not considerably increase for the smaller inclusions: e.g. for the $1.2\,cm$ inclusion the error was $0.2\,cm$ in sound speed and $0.2\,cm$ in attenuation.

Figure 3 shows a maximum intensity projection of the bonding wire imaged with reflection tomography. For this overview image the resolution was reduced to approximately $1.5\,mm$. At the indicated locations we reconstructed small sub volumes with a resolution of approximately $0.1\,mm$. The average FWHM in these sub volumes along the x-,y- and z-axis was $0.24\,mm \pm 0.05\,mm$, $0.27\,mm \pm 0.08\,mm$ and $0.27\,mm \pm 0.08\,mm$ respectively.

In figure 4 we compare a reflectivity reconstruction of the same healthy volunteer with USCT II (top) and USCT III (bottom). Visually it can be recognized that the breast tissue up to the chest wall can be imaged with USCT III with better contrast. Inner structures appear with more contrast and grating lobe artifacts at the breast surface are suppressed. Quantitatively, the positioning of the mamilla below the upper most transducer was $32\,mm$ for USCT II and $68\,mm$ for USCT III respectively, which indicates that considerably more tissue is within the region of interest in which the best illumination and contrast can be expected. Also for transmission tomography, this means that considerably more breast tissue can be imaged since due to the ray assumption only the tissue inside the area covered by transducers can be reconstructed (Figure 5).

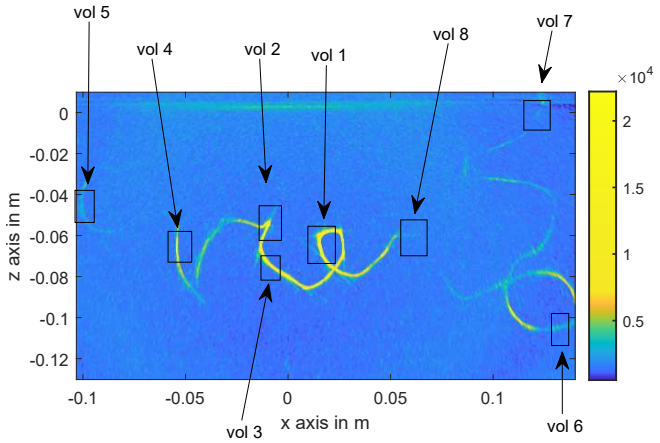

Figure 3: Maximum intensity projection of the reflection reconstruction showing the twisted bonding wire. The annotations indicate the locations, at which sub-volumens with high resolution have been reconstructed to assess the PSF.

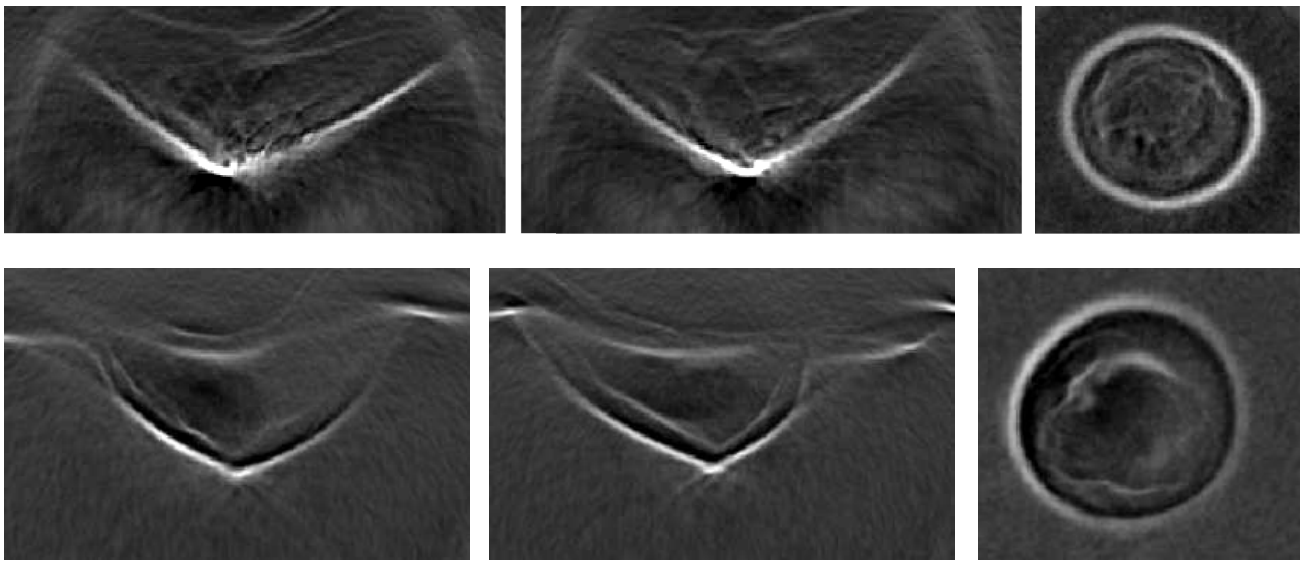

Figure 4: Reflection reconstructions of volunteer scans with USCT II (top) and USCT III (bottom).

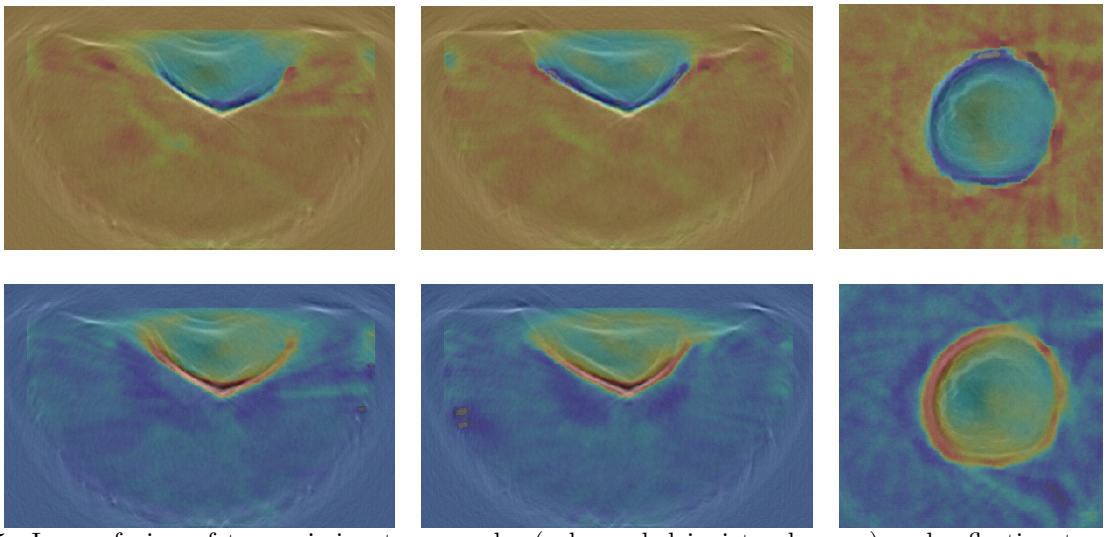

Figure 5: Image fusion of transmission tomography (color-coded in jet colormap) and reflection tomography (gray scale background). The top row shows the image fusion of sound speed and reflection, the bottom row shows the image fusion of attenuation and reflection. From left to right a transversal, sagittal and coronal plane is depicted.

4. DISCUSSION AND CONCLUSION

In this paper we present a first analysis of the imaging capabilities of the world's first 3D Ultrasound Tomography system with pseudo-random sampling. While the system at KIT is still in commissioning phase, i.e. undergoing calibration, the results are already promising. E.g. the contrast is considerably improved in reflectivity imaging (Fig. 4). The breast is immersed considerably deeper in the water, thereby the entire volume up to the breast muscle can be imaged. Together with an increased opening angle of the transducers this leads to a considerable improvement of both the reflection images and the transmission images, the latter despite the use of still simple ray based methods.

Quantitatively the transmission imaging results obtained with phantom data show a deviation of less than $5\,m/s$ and $0.2\,dB/cm$ for the phantom body and less than $15\,m/s$ and $0.2\,dB/cm$ for the largest inclusion. Considering the standard deviation of the ground truth measurements we conclude that this is a good agreement. Geometric errors are in average in the range of $0.2\,cm$. In reflectivity imaging we could show that the PSF is nearly isotropic and with an average of $0.26\,mm$ close to the USCT II system[8] and the predictions for the current system.[9]

In our ongoing work we are focusing on a more complete calibration and characterization of the USCT III system which we expect to improve the image quality further. Along this ongoing work we will image more phantom data to increase statistical significance and further volunteers before entering a clinical study.

REFERENCES

[1] Littrup, P. J., Duric, N., Sak, M., Li, C., Roy, O., Brem, R. F., Larsen, L. H., and Yamashita, M., "Multicenter study of whole breast stiffness imaging by ultrasound tomography (SoftVue) for characterization of breast tissues and masses," *Journal of Clinical Medicine* **10**(23), 5528 (2021).

[2] Malik, B., Iuanow, E., and Klock, J., "An exploratory multi-reader, multi-case study comparing transmission ultrasound to mammography on recall rates and detection rates for breast cancer lesions," *Academic Radiology* **29**, S10–S18 (2022).

[3] Ruiter, N., Zapf, M., Dapp, R., Hopp, T., Kaiser, W., and Gemmeke, H., "First results of a clinical study with 3D ultrasound computer tomography," in [*2013 IEEE International Ultrasonics Symposium (IUS)*], IEEE (2013).

[4] Zapf, M., Hopp, T., Gemmeke, H., Angerer, M., Lu, Z., Molchanova, O., Rashvand, N., Blanco, R., Steck, P., Leyrer, B., Tcherniakhovski, D., Bormann, D., Schlote-Holubek, K., and Ruiter, N. V., "Realization of an pseudo-randomly sampled 3D USCT," in [*Medical Imaging 2022: Ultrasonic Imaging and Tomography*], Ruiter, N. V. and Bottenus, N., eds., SPIE (2022).

[5] Li, C., *Compressive Sensing for 3D Data Processing Tasks:Applications, Models and Algorithms*, PhD thesis, Rice University, Houston, US (2011).

[6] Ruiter, N. V., Kretzek, E., Zapf, M., Hopp, T., and Gemmeke, H., "Time of flight interpolated synthetic aperture focusing technique," in [*SPIE Proceedings*], SPIE (2017).

[7] Angerer, M., Zapf, M., Koppenhofer, J., and Ruiter, N. V., "Method to extract frequency dependent material attenuation for improved transducer models," in [*2021 IEEE International Ultrasonics Symposium (IUS)*], 1–4 (2021).

[8] Gemmeke, H., Hopp, T., Zapf, M., Kaiser, C., and Ruiter, N. V., "3d ultrasound computer tomography: Hardware setup, reconstruction methods and first clinical results," *Nuclear Instruments and Methods in Physics Research Section A: Accelerators, Spectrometers, Detectors and Associated Equipment* **873**, 59–65 (2017). Imaging 2016.

[9] Gemmeke, H., Berger, L., Hopp, T., Zapf, M., Tan, W., Blanco, R., Leys, R., Peric, I., and Ruiter, N. V., "The new generation of the kit 3d usct," in [*Proceedings of the International Workshop on Medical Ultrasound Tomography: 1.- 3. Nov. 2017, Speyer, Germany*], 271–282, KIT Scientific Publishing (2018).